IOPscience iopscience.iop.org

Home Search Collections Journals About Contact us My IOPscience

An electron-spin-resonance study of substitutional disorder in Ce^{3+}-doped $CaYAlO_4$

This article has been downloaded from IOPscience. Please scroll down to see the full text article.

1997 J. Phys.: Condens. Matter 9 9639

(http://iopscience.iop.org/0953-8984/9/44/018)

View the table of contents for this issue, or go to the journal homepage for more

Download details:
IP Address: 171.66.16.209
The article was downloaded on 14/05/2010 at 10:57

Please note that terms and conditions apply.

J. Phys.: Condens. Matter **9** (1997) 9639–9649. Printed in the UK PII: S0953-8984(97)84832-1

An electron-spin-resonance study of substitutional disorder in Ce^{3+}-doped $CaYAlO_4$

M Yamaga†, N Kodama‡, T Yosida§, B Henderson‖ and K Kindo¶

† Department of Electronics, Faculty of Engineering, Gifu University, Gifu 501-11, Japan
‡ Department of Chemistry, Faculty of Education, Akita University, Akita 010, Japan
§ Nakanihon Automotive College, Kamo 505, Japan
‖ Department of Physics and Applied Physics, University of Strathclyde, Glasgow G1 1XN, UK
¶ Research Centre for Extreme Materials, Osaka University, Toyonaka 560, Japan

Received 3 June 1997

Abstract. Electron spin-resonance (ESR) spectra of Ce^{3+} ions in $CaYAlO_4$ (CYA) crystals have been measured at X-band microwave frequency. The spectra are only observed below 50 K: they are very broad and easily saturated by low microwave power at 4.2 K. The ESR lines, which vary in position with orientation of the magnetic field relative to the crystalline axes, have been fitted to a tetragonal spin Hamiltonian with the principal components ($g_\parallel$, $g_\perp$) observed to be close to those of Ce^{3+} ions in $CaWO_4$ and $LiYF_4$. The associated microwave absorption is due to the lowest crystal-field level of the $^2F_{5/2}$ ground state of the Ce^{3+} ion in CYA. The measured g-tensor components $g_\parallel = 2.52(2)$ and $g_\perp = 1.54(2)$ for Ce^{3+} in CYA can be explained in terms of the ground-state wavefunction composed of $|j, j_z\rangle = |5/2, \pm 5/2\rangle$ and $|5/2, \mp 3/2\rangle$ components of $^2F_{5/2}$ mixed by the crystal-field terms $B_4^4 O_4^4$ and $B_6^4 O_6^4$.

The inhomogeneous broadening of the asymmetric ESR lines reflects a distribution of g-values, which is produced by tilting the principal z-axis of the Ce^{3+} effective spin away from the crystal c-axis and a distribution of the ground-state spin levels in $^2F_{5/2}$ of the Ce^{3+} ions through the random occupation of Ca^{2+}/Y^{3+} ions at the appropriate site in the disordered CYA lattice.

1. Introduction

There is much current interest in Ce^{3+}-doped ionic crystals for potential applications in UV lasers and scintillators [1–3]. The electronic configuration of the Ce^{3+} ground state is $4f^1$, whereas that of the excited state is $5d^1$. The 4f ↔ 5d transitions, which occur by allowed electric dipole processes, have large transition probabilities. Since the electron–phonon couplings of the 4f and 5d electrons are quite different, the 4f ↔ 5d transitions feature broad absorption and emission bands with a large Stokes shift between them. This gives rise potentially to broad tuning ranges for laser oscillation. Recently, the operation of an optically pumped, tunable solid-state laser using the 4f ↔ 5d transition of Ce^{3+} in $LiYF_4$ at room temperature was reported [4].

In an earlier paper [5], the authors reported the optical properties of Ce^{3+} in $CaYAlO_4$ (CYA). The inhomogeneous broadening of the Ce^{3+} luminescence is caused by *substitutional disorder* of the Ca^{2+}/Y^{3+} sites in the CYA lattice. This phenomenon was first discussed for Cr^{3+}-doped CYA crystals [6, 7], where it was established that the *substitutional disorder* created variations in the crystal-field strength at the Cr^{3+} ion sites, and that this gave rise to distributions in the positions of the ground and excited energy levels. Electron spin

0953-8984/97/449639+11$19.50 © 1997 IOP Publishing Ltd

resonance (ESR) in the Ce^{3+} ground state reveals the local structure of the Ce^{3+} ion and the distribution of observed g-values in the disordered crystal. This paper discusses the surrounding environment of Ce^{3+} and the mixing of the $^2F_{5/2}$ ground-state wavefunctions in the disordered crystal, as determined from the inhomogeneously broadened ESR spectra.

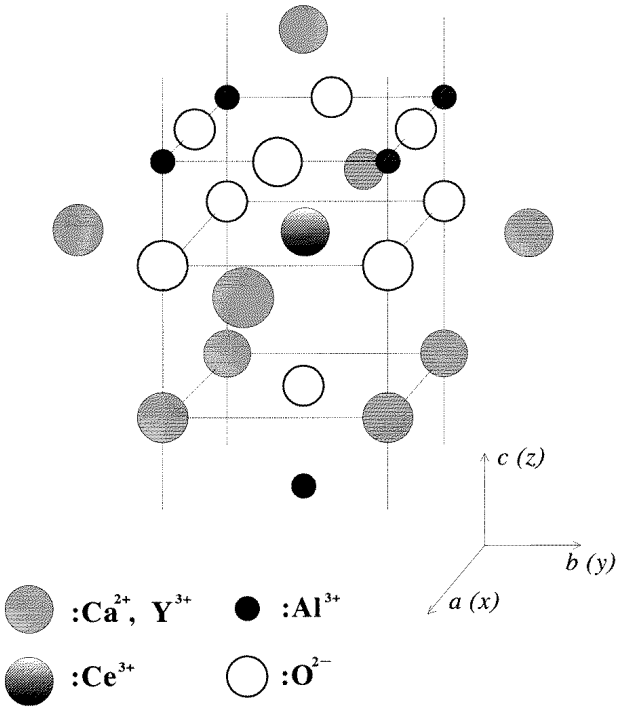

Figure 1. A part of the unit cell of the crystal structure of $CaYAlO_4$

2. Experimental details

The crystal structure of CYA belongs to the space group $I4/mmm$ (D_{4h}^{17}). The lattice constants are $a = b = 3.6451$ Å and $c = 11.8743$ Å [8, 9]. Figure 1 shows a part of the unit cell centred on one of the Ca^{2+}/Y^{3+} sites. Ca^{2+} and Y^{3+} ions are randomly distributed on their common lattice site, the Ca^{2+}/Y^{3+} composition ratio of 1:1 being maintained to retain the bulk crystal composition ($CaYAlO_4$) of the crystal. The Ce^{3+} ions are expected to occupy preferentially the Ca^{2+}/Y^{3+} sites [5]. In consequence, they are surrounded by nine nearest-neighbour oxygen ligand ions, four next-nearest-neighbour Ca^{2+}/Y^{3+} ions in the ab-plane containing the Ce^{3+} ions and five next-nearest-neighbour Ca^{2+}/Y^{3+} ions out of this plane as shown in figure 1. The random occupation of Ca^{2+}/Y^{3+} ions causes random perturbations of the electrostatic crystal field at the Ce^{3+} ions, and in consequence, to the crystal-field Hamiltonian. Therefore, the symmetry of the surrounding is different at each site.

The CYA crystals were grown by the Czochralski technique as described in reference [5]. The concentrations of Ce^{3+} relative to Y^{3+} in the CYA melt are 0.5 and 5 at.%. The dimensions of the experimental samples were $4 \times 4 \times 2$ mm^3, with faces cut parallel to the

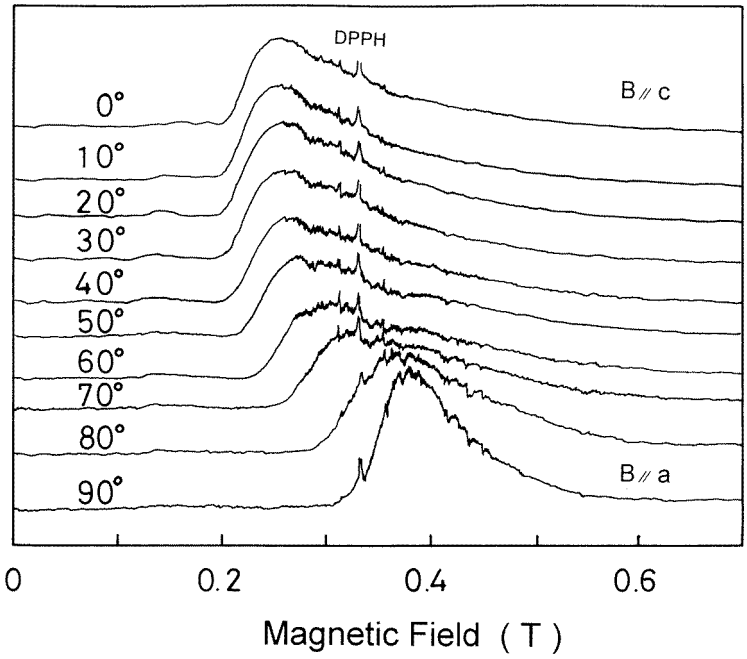

Figure 2. The orientation dependence of the ESR spectra of Ce^{3+}(0.5%) in CYA with the magnetic field applied in the *ac*-plane measured at 4.2 K and a microwave frequency of 9.370 GHz.

(100), (010) and (001) planes.

The ESR measurements were made at temperatures in the range 4.2–50 K using a Varian X-band spectrometer equipped with 270 Hz field modulation, as described by the authors' colleagues in reference [10].

3. Experimental results

Figure 2 shows the ESR spectra in Ce(0.5%):CYA measured at 4.2 K with the magnetic field applied in the *ac*-plane. For these spectra the microwave frequency was 9.370 GHz and 0.2 mW of microwave power was incident upon the cavity. The full range of the available magnetic field of 0–1 T was swept through in two minutes. The signal of the DPPH field marker is observed at ∼0.332 T. Only the broad, positive part of a derivative line appears on the low-magnetic-field side of Ce-impurity resonances, when sweeping from low magnetic field to high field. The peak of the resonance, which shifts from low field to high field when the magnetic field is rotated from the *c*- to the *a*-axis, remains constant in the *ab*-plane (not shown).

These broad ESR signals do not change in shape or intensity when the microwave power is varied in the range 0.05–1 mW, indicating that the ESR transitions are easily saturated at 4.2 K. The intensities of the spectra decrease rapidly when the sweep rate ($\mathrm{d}B/\mathrm{d}t$) over the full 0–1 T range of the variable magnetic field is decreased; they are not detected when the rate is less than 1 mT s^{-1}. Figure 3 shows the ESR spectra at 4.2 K with $\boldsymbol{B} \parallel \boldsymbol{c}$: the field was swept both down to low and up to high field, through resonance, at a rate

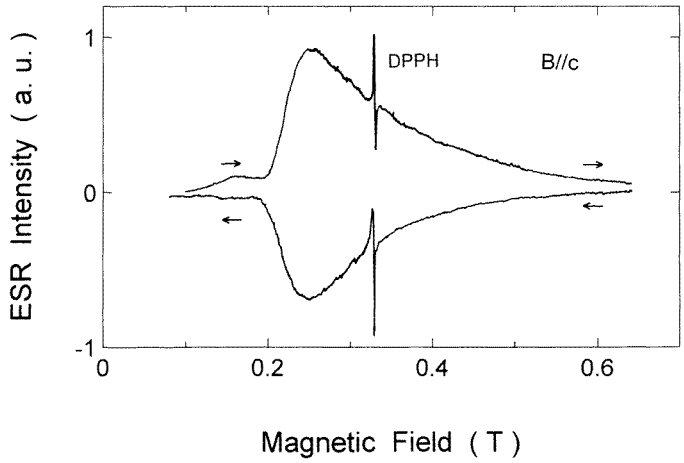

Figure 3. The ESR spectra of Ce^{3+}(0.5%) in CYA with $\boldsymbol{B} \parallel \boldsymbol{c}$ on sweeping the field down and up through resonance.

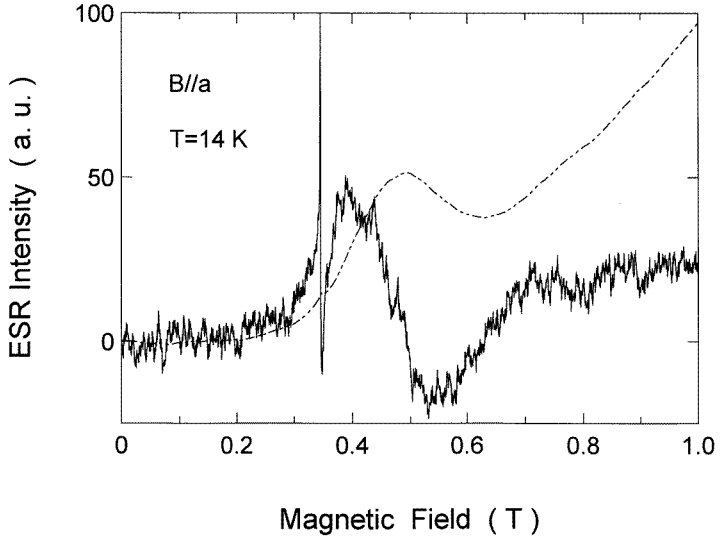

Figure 4. The ESR spectrum of Ce^{3+}(0.5%) in CYA at $T = 14$ K and with $\boldsymbol{B} \parallel \boldsymbol{a}$. The solid and chain curves represent the first derivative and integrated spectra, respectively.

of 8.3 mT s^{-1}. Although the traces are reversed with respect to each other, the line shape with a long tail decreasing towards higher field does not change. Such phenomena occur for resonances measured under conditions of adiabatic rapid passage, in which the sweep rate is much faster than the spin–lattice relaxation rate [11].

When the temperature is increased above 4.2 K, the line shapes of the ESR spectra change. The negative components of the expected derivative signals begin to appear at high magnetic field. The ESR spectrum observed at 14 K with $\boldsymbol{B} \parallel \boldsymbol{a}$ is almost symmetric, as shown in figure 4. For $\boldsymbol{B} \parallel \boldsymbol{c}$ the weak negative signal appears on the high-magnetic-field

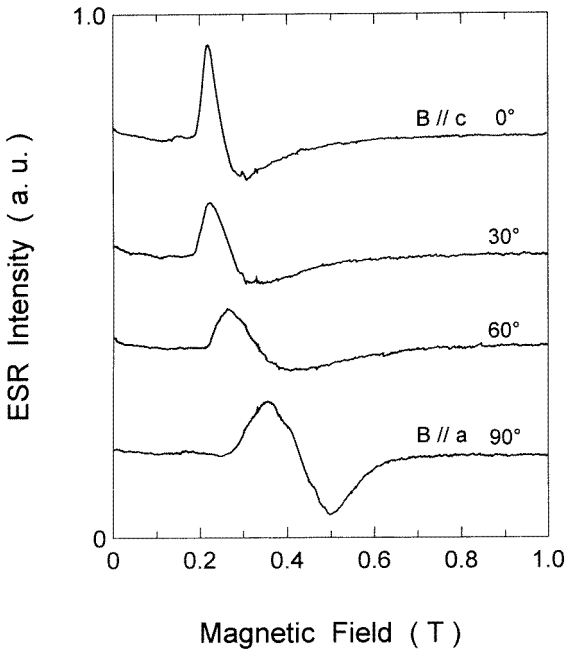

Figure 5. The orientation dependence of the ESR spectra of Ce^{3+}(5%) in CYA with the magnetic field applied in the *ac*-plane measured at 4.2 K and a microwave frequency of 9.246 GHz.

side of the line. The observed line shape is still asymmetric. Above 40 K, the peak-to-peak intensities of the spectra with $\boldsymbol{B} \parallel \boldsymbol{a}, \boldsymbol{c}$ are not detectable because of line broadening. Such a temperature dependence suggests that the spin–lattice relaxation rate is enhanced at higher temperatures and that the line broadening is induced by an Orbach process [10].

Figure 5 shows the ESR spectra in Ce(5%):CYA at 4.2 K with the magnetic field applied in the *ac*-plane. The microwave frequency was 9.246 GHz, the microwave power was 0.5 mW, and the sweep rate was 4 mT s^{-1}. The ESR signals, which were not saturated below 0.5 mW of microwave power, are in the form of the first derivative of an absorption peak, being composed of positive and negative parts. The resonance field shifts from low field to high field when the magnetic field is rotated from the *c*- to the *a*-axis as in the case of Ce(0.5%):CYA. The line shape with $\boldsymbol{B} \parallel \boldsymbol{c}$ has a long tail towards higher field. On the other hand, with $\boldsymbol{B} \parallel \boldsymbol{a}$ it is symmetric, being the same as that observed for Ce(0.5%):CYA at 14 K in figure 4. The difference between the ESR spectra of Ce(0.5%) and Ce(5%) in CYA measured at 4.2 K may be explained by relaxation effects of these Ce^{3+} Kramers doublets, which are represented by the sums of longitudinal and transverse relaxation rates. The longitudinal rate corresponds to spin–lattice interaction, whereas the transverse rate corresponds to spin–spin interaction. The ESR results suggest that the spin–lattice relaxation rates at 4.2 K for both crystals are smaller than the field sweep rate divided by an amplitude of oscillatory magnetic field and that the spin–spin interaction for Ce(5%):CYA, being independent of temperature, is enhanced by the high concentration of Ce^{3+} ions.

In order to examine the relaxation effect, the ESR line shapes for the two crystals have been compared with each other. The upper part of figure 6 shows the first derivative (solid line) of the microwave absorption for the Ce(0.5%):CYA sample. The lower part shows the first derivative (solid line) and the integral (dot–dashed line) of the derivative signal, which is equal to the microwave absorption in Ce(5%):CYA. The fact that the integrated

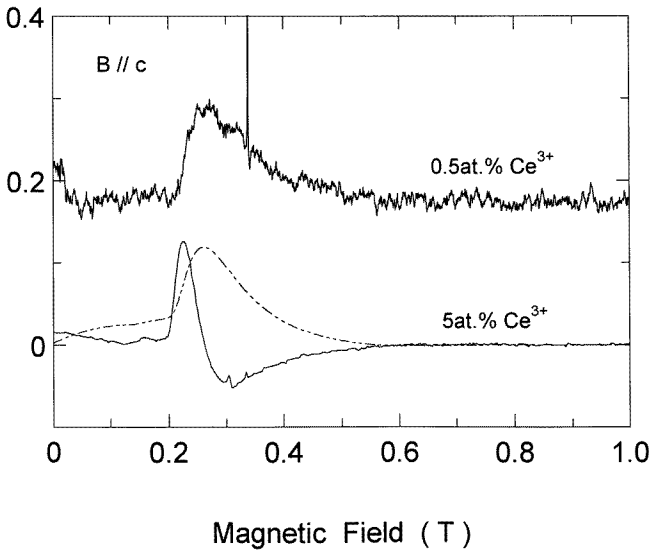

Figure 6. The comparison with the ESR spectra of Ce^{3+} (0.5%) and Ce^{3+} (5%) in CYA with $\boldsymbol{B} \parallel \boldsymbol{c}$. The full curves represent the first derivative and the dot–dashed curve was calculated by integrating the derivative signal.

spectrum for Ce(5%):CYA is in agreement with the derivative for Ce(0.5%):CYA can be explained by the relaxation process between two spin sublevels of Ce^{3+}. The ESR spectrum in Ce(0.5%):CYA may be inhomogeneously broadened. In that case, an individual resonance line for each Ce^{3+} ion forms as a positive (or negative) part of the first-derivative signal, because at 4.2 K the spin–lattice relaxation rate is smaller than the field sweep rate. In consequence, the observed ESR spectrum being associated with the envelope function of the resonances from all of the ions is fairly close to a microwave absorption spectrum, as shown in figure 6.

Figure 7 shows the temperature dependence of the ESR spectra with $\boldsymbol{B} \parallel \boldsymbol{c}, \boldsymbol{a}$ for Ce(5%):CYA in the range 6–50 K. The peak-to-peak intensities of the ESR lines decrease rapidly with increasing temperature such that they are not detected above $T_{dis} = 50$ K. These trends are caused by the temperature dependence of the spin–lattice relaxation rate, which determines the linewidth. The linewidth, $\Gamma(T)$, is given by

$$\Gamma(T) = a + bT + cT^n + d\Delta^3 \exp(-\Delta/kT) \tag{1}$$

where Δ is the energy separation of the lowest-lying excited electronic state from the ground state and $a, b, c,$ and d are constants [12, 13]. The first term, a, in equation (1) represents inhomogeneous broadening independent of T. The second, third, and fourth terms are due to the direct, the Raman, and the Orbach processes, respectively. The Orbach process is very important for the broadening of the ESR spectra of rare-earth ions except Gd^{3+} and Eu^{2+} ions, which can be measured only at low temperature. The activation energy, Δ, is estimated from the temperature dependence of the ESR linewidth. The values of T_{dis} and Δ for Ce^{3+} in $LiYF_4$ were reported to be 50 K and 175 cm^{-1}, respectively, on the assumption that the second and third terms in equation (1) are negligible [10]. T_{dis} for CYA is $\sim$50 K. It is difficult to derive the temperature dependence of the linewidth from the spectrum shown in figure 7 because of the large inhomogeneous width. However, Δ is estimated

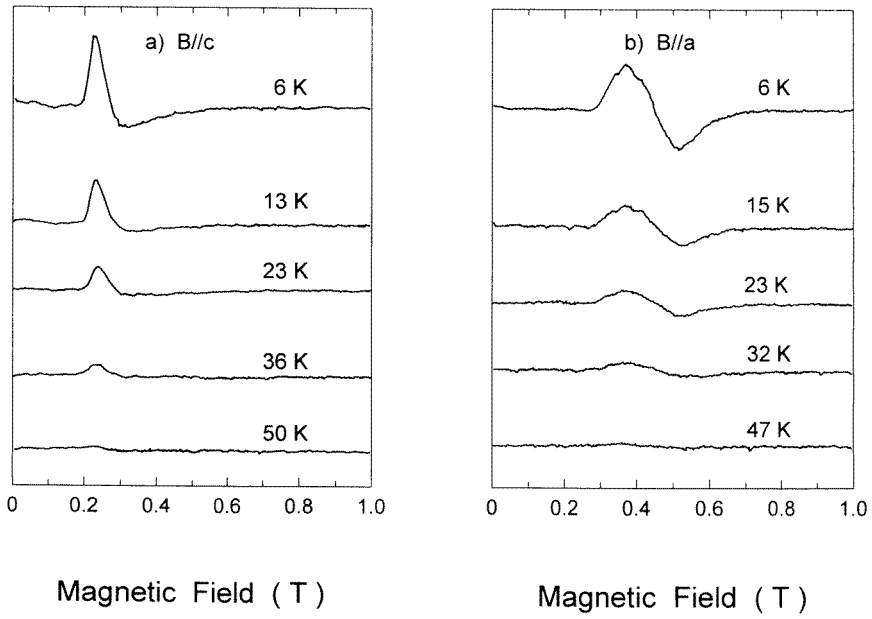

Figure 7. The temperature dependence of the ESR spectra of Ce^{3+} (5%) in CYA with (a) $\boldsymbol{B} \parallel \boldsymbol{c}$ and (b) $\boldsymbol{B} \parallel \boldsymbol{a}$ in the range 6–50 K.

to be $\sim$150 cm^{-1} from T_{dis} $\sim$50 K, by comparison with the case of Ce^{3+} in $LiYF_4$. The energy separation of the lowest-lying excited state is much larger than the energy of the X-band microwave quantum ($\sim$0.3 cm^{-1}). In consequence, the inhomogeneous broadening of the ESR spectrum may be due not to unresolved fine structure, but to a distribution of g-values, caused by mixing between the electronic states of $^2F_{5/2}$ induced through the random occupation of Ca^{2+}/Y^{3+} ions.

The ESR lines of Ce^{3+} in CYA can be analysed by using an effective spin Hamiltonian with tetragonal symmetry:

$$\mathcal{H} = \mu_B g_\parallel H_z S_z + \mu_B g_\perp (H_x S_x + H_y S_y) \tag{2}$$

with an effective spin $S = 1/2$, where μ_B is the Bohr magneton. The principal z-, x-, and y-axes are parallel to the crystal c-, a-, and b-axes, respectively. The observed mean g-values ($g_\parallel = 2.52$, $g_\perp = 1.54$) for Ce(5%):CYA are quite close to those of Ce^{3+} in $CaWO_4$ ($g_\parallel = 2.91$, $g_\perp = 1.42$) [14] and in $LiYF_4$ ($g_\parallel = 2.765$, $g_\perp = 1.473$) [10], both crystals with tetragonal S_4 symmetry. The distributions of g-values for $\boldsymbol{B} \parallel \boldsymbol{c}, \boldsymbol{a}$ are estimated from the inhomogeneous linewidths using the relationship of $h\nu = \mu_B g B$ and range approximately from 1.2 to 3.3 and from 1.0 to 2.0, respectively.

4. Discussion

4.1. The wavefunction of the $^2F_{5/2}$ ground state

The Ce^{3+} ion in its lowest energy state has a single 4f electron outside the closed shells, and the $^2F_{5/2}$ ground state is separated from the lowest-lying excited state $^2F_{7/2}$ by the spin–orbit energy of approximately 2000 cm^{-1}. The g-tensor of Ce^{3+} may be understood

in terms of the wavefunction of the $^2F_{5/2}$ ground state, which is split into three Kramers doublets by the crystal field. The crystal-field Hamiltonian for tetragonal symmetry (S_4) is

$$\mathcal{H}_{cry} = B_2^0 O_2^0 + B_4^0 O_4^0 + B_4^4 O_4^4 + B_6^0 O_6^0 + B_6^4 O_6^4 + B_6^6 O_6^6 \tag{3}$$

where the O_n^m are equivalent spin operators and the B_n^m are experimentally determined constants [13, 15]. In LS-coupling, the electronic states are characterized by four quantum numbers j, j_z, l, and s, where $\boldsymbol{j} = \boldsymbol{l} + \boldsymbol{s}$. As the $4f^1$ configuration of Ce^{3+} has $l = 3$ and $s = 1/2$, the eigenfunction is simply denoted by $|j, j_z\rangle$. The eigenfunctions of a crystal-field Hamiltonian with axial symmetry, which includes only the terms $B_n^0 O_n^0$, are represented by $|j, j_z\rangle = |5/2, \pm 1/2\rangle, |5/2, \pm 3/2\rangle, |5/2, \pm 5/2\rangle$. The g-values are calculated to be $(g_\parallel, g_\perp) = (g_L, 3g_L)$, $(3g_L, 0)$, and $(5g_L, 0)$ where g_L (=6/7) is the Landé factor for the $j = 5/2$, using $|5/2, \pm 1/2\rangle$, $|5/2, \pm 3/2\rangle$, and $|5/2, \pm 5/2\rangle$, respectively [13, 15]. The agreement between the calculated and measured values ($g_\parallel = 2.52$, $g_\perp = 1.54$) is not very good.

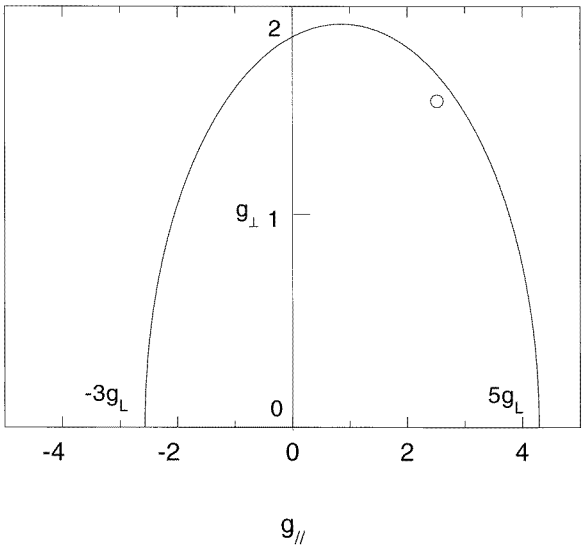

Figure 8. The relationship between $g_\parallel$ and $g_\perp$ calculated using equation (5). An open circle represents experimental g-values ($g_\parallel = 2.52$, $g_\perp = 1.54$) of Ce^{3+}(5%) in CYA.

In order to resolve this discrepancy, the effects of the crystal-field terms $B_4^4 O_4^4$ and $B_6^4 O_6^4$ which mix the $|5/2, \pm 5/2\rangle$ and $|5/2, \mp 3/2\rangle$ spin states are considered. The g-value is then calculated by the method used in the case of Ce^{3+} in $CaWO_4$ [15]. The wavefunction of the $^2F_{5/2}$ ground state is assumed to be

$$\left|\frac{5}{2}, \pm\frac{5'}{2}\right\rangle = \cos\theta \left|\frac{5}{2}, \pm\frac{5}{2}\right\rangle + \sin\theta \left|\frac{5}{2}, \mp\frac{3}{2}\right\rangle \tag{4}$$

and gives the resulting g-values of

$$\begin{aligned} g_\parallel &= g_L(8\cos^2\theta - 3) \\ g_\perp &= g_L(2\sqrt{5}\cos\theta\sin\theta). \end{aligned} \tag{5}$$

Figure 8 shows the relationship between $g_\parallel$ and $g_\perp$ calculated using equation (5), the parameter θ being varied from 0 to $\pi/2$. Also shown is the data point ($g_\parallel = 2.52$,

$g_\perp = 1.54$). The absolute values of the solution of equation (5) are associated with the experimental g-values. The pair of values $g_\parallel = 2.67$ and $g_\perp = 1.62$ in the graphical solution to equation (5) and calculated with $\theta = 29^\circ$ give a close fit to the measured values. The fact that the dominant component of the $^2F_{5/2}$ ground state is approximately $|5/2, \pm 5/2\rangle$ suggests that the diagonal matrix elements of $(B_2^0 O_2^0 + B_4^0 O_4^0 + B_6^0 O_6^0)$ between the wavefunctions of $^2F_{5/2}$ are larger than the off-diagonal matrix elements of $(B_4^4 O_4^4 + B_6^4 O_6^4)$ and that the crystal-field parameter B_2^0 must be negative.

4.2. The inhomogeneous broadening of the ESR lines

The authors have previously discussed the inhomogeneous broadening by disorder of the Cr^{3+} ESR lines observed in CYA [7]. The ESR spectra were composed of the lines assigned to Cr^{3+} ions at ordered and disordered sites, where the principal axes were parallel to the crystal axes and tilted from the crystal axes, respectively. The low-symmetry disordered configurations correspond to a random occupation of eight second-nearest-neighbour Ca^{2+}/Y^{3+} ions of the central Cr^{3+} ion. Although the Ce^{3+} ions occupy different sites from the Cr^{3+} ions, the inhomogeneous broadening of the ESR line can be discussed assuming the same model for Ce^{3+}:CYA as for Cr^{3+}:CYA.

In CYA, Ca^{2+} and Y^{3+} ions are randomly distributed on their common lattice sites illustrated in figure 1. If the four cations in each separate parallel ab-plane are Ca^{2+} (Y^{3+}) ions, these ordered configurations show tetragonal symmetry along the c-axis. However, when one of the four Ca^{2+} (Y^{3+}) cations in each ab-plane is exchanged with the other Y^{3+} (Ca^{2+}), while keeping the number ratio (4:4) of Ca^{2+} and Y^{3+} constant, sixteen disordered configurations are produced, which can be classified into two distinct groups of eight equivalent configurations. If two cations are exchanged between the two planes, there are 144 distinct disordered configurations, which are classified into several groups. Such disordered configurations lower the symmetry of the surrounding, and cause the principal axes of Ce^{3+} ion to be tilted away from the crystalline axes. The tilting is strongly related to the magnitude of the crystal-field operators $B_n^m O_n^m$ $(m \neq 0)$, which mix the wavefunctions in $^2F_{5/2}$ and $^2F_{7/2}$ into the lowest ground state. The mixing introduces a distribution in the g-values. In consequence, the inhomogeneous broadening of the ESR lines observed with $\boldsymbol{B} \parallel \boldsymbol{c}, \boldsymbol{a}$ is due to the tilting of the principal-axis system and the distribution of the g-values.

Since it is difficult to describe quantitatively the relationship between the tilting and the g-value distribution, their effects are considered separately. It is assumed that the inhomogeneous broadening is caused by the tilting of the principal z-axis of Ce^{3+} away from the c-axis with fixed anisotropic g-factors ($g_\parallel$, $g_\perp$). Defining the tilting angle of one disordered configuration as ψ, the g-value of the Ce^{3+} ion, when the applied magnetic field is parallel to the c-axis, is given by

$$g^2 = g_\parallel^2 \cos^2 \psi + g_\perp^2 \sin^2 \psi. \tag{6}$$

The lineshape of the powder-like ESR spectrum as a function of the magnetic field is calculated assuming that the principal axis is tilted uniformly through an angle in the range 0–$\pi/2$, and transformed using equation (6) and $h\nu = \mu_B g B$. The calculation shows that the spectrum should have a finite step at $B_\parallel$, followed by a gradual increase towards $B_\perp$, reaching an infinite value at $B_\perp$ [12, 13]. The difference between the observed ESR spectrum with $\boldsymbol{B} \parallel \boldsymbol{c}$ and the expected powder-like spectrum is the lack of the strong signals at $g_\perp$ in the observed spectrum. In consequence, the principal axis of Ce^{3+} is expected to be tilted through an angle that is finite but less than $\pi/2$ away from the c-axis. The angle is roughly

estimated to be in the range of 0–50° from the overlap of the spectra with $\boldsymbol{B} \parallel \boldsymbol{c}$ and $\boldsymbol{B} \parallel \boldsymbol{a}$ on the assumption that $g_{\parallel} = 2.5$ and $g_{\perp} = 1.6$. This value is much larger than that obtained from the ESR results for Cr^{3+} in CYA ($\psi \leqslant 20°$) [7]. There is also the question of why the $\boldsymbol{B} \parallel \boldsymbol{a}$ spectrum has neither a steep rise on the higher-field side nor a long tail towards lower field as for the $\boldsymbol{B} \parallel \boldsymbol{c}$ spectrum.

Now consider a distribution of the g-values of the disordered configurations with the axis of distortion along the c-axis. Figure 8 shows that when the angle θ in equations (5) varies from 22° to 42°, the $g_{\parallel}$- and $g_{\perp}$-values are in the ranges 3.3–1.2 and 1.3–1.9, respectively. This accounts for the observed ranges, $g_{\parallel} \sim 1.2$–3.3 and $g_{\perp} \sim 1.0$–2.0, and for the distribution of $g_{\parallel}$ being much wider than that of $g_{\perp}$. The comparison of the observed distributions in the g-values in these two cases suggests that the contribution of the mixing of the wavefunctions is dominant. As the mixing occurs through lowering of the symmetry of the Ce^{3+} environment, the tilting of the principal axes cannot be neglected, even though it is not possible to distinguish the separate contributions from the observed ESR line shape.

4.3. Spin–spin interaction

In substitutionally disordered CYA crystals, spin–lattice relaxation between the spin sublevels of Ce^{3+} may be slower than in regular crystals such as $LiYF_4$ [10]. In consequence, the ESR signal observed for Ce(0.5%):CYA at 4.2 K is only the positive part of the first derivative, because the relaxation rate is small compared with the field sweep rate. The spin–lattice relaxation rate increases abruptly with increasing temperature, such that at 14 K, the ESR spectrum with $\boldsymbol{B} \parallel \boldsymbol{a}$ becomes symmetrical. In contrast, the ESR spectrum for $\boldsymbol{B} \parallel \boldsymbol{a}$ of Ce(5%):CYA is symmetric even at 4.2 K, the relaxation rate being enhanced by spin–spin interaction at the higher Ce^{3+} concentration. It is appropriate to discuss the ESR line shape in terms of spin–spin interaction.

The simplest type of spin–spin interaction is the magnetic dipole interaction between two neighbouring paramagnetic ions for low concentrations of impurity ions in crystals. If the paramagnetic ions are identical, they precess at the same frequency in the external magnetic field. The neighbouring paramagnetic ions are coupled through their precessing components of magnetic dipoles, and the exchanges of quanta occur between the ions. This interaction additionally broadens the resonance line and shortens the lifetime of the spin sublevels of the ions. This lifetime is related to a spin–spin relaxation time T_2, which corresponds to homogeneous broadening through the relation $T_2 = 1/(2\pi\,\Delta\nu)$. On increasing the concentration of the paramagnetic ions, the probability of pairs of ions occupying near-neighbour sites increases. When the separation between the pair of ions is decreased to less than $\simeq$0.5 nm, the strength of the exchange interaction between neighbours is enhanced sufficiently that it exceeds the magnetic dipole interaction. This is a temperature-independent interaction, which is not supported by the present results over the rather restricted temperature range. Nor is it expected that exchange will dominate at the concentration of Ce^{3+} in the present crystals.

The probability that one of nine nearest-neighbour Ca^{2+}/Y^{3+} sites of a central Ce^{3+} is replaced by another Ce^{3+} ion is 0.02 and 0.17 for Ce(0.5%):CYA and Ce(5%):CYA, respectively, assuming charge neutrality and random occupation by five Ca^{2+}, three Y^{3+}, and two Ce^{3+} ions including the central Ce^{3+} ion for the local structure shown in figure 1. Since the real concentrations of Ce^{3+} in the CYA crystals are less than those quoted (i.e. 0.5%, 5%) for the melt, because of the coexistence of Ce^{3+} and Ce^{4+} in the crystal, the actual probability for Ce(5%):CYA will be less than 0.17. This will be further diminished by

equally high probability that the central Ce^{3+} ion will have another Ce^{3+} ion in the third- or fourth-nearest-neighbour Ca^{2+}/Y^{3+} sites. In consequence, although the spectrum in Ce(5%):CYA includes contributions from the magnetic dipole and exchange interactions, the dominant component of the signal for the Ce(5%):CYA will be due not to the pair but to the isolated Ce^{3+} ions.

The integrated line shape of the first derivative observed for Ce(5%):CYA is close to the first derivative for Ce(0.5%):CYA on the assumption that the positive part of an individual resonance line of each Ce^{3+} ion under conditions of adiabatic rapid passage is proportional to the intensity of the microwave absorption. Taking account of these results, the line shapes of the microwave absorption spectra for the two crystals are expected to be almost identical. It is concluded that Ce^{3+} ions in CYA interact through the magnetic dipole, enhancing the spin–spin relaxation rate between the spin sublevels of Ce^{3+}, with the result that the first derivative is observed at 4.2 K for the Ce(5%):CYA crystals.

5. Conclusions

The mean g-values ($g_{\parallel} = 2.52, g_{\perp} = 1.54$) of Ce^{3+} in the disordered CYA crystal measured by ESR studies show that the local environment has tetragonal symmetry with a negative crystal-field parameter B_2^0. The inhomogeneous broadening of the ESR spectrum is associated with the distribution of the g-values, which is created by distributions of both the tilting angle of the principal axis and the energy separation of the $^2F_{5/2}$ ground state.

Acknowledgments

The work was supported by a Grant-in-Aid for Scientific Research on the Priority Area ‘New Development of Rare Earth Complexes’ (Nos 07230233, 08220228) and on Areas (C) (No 07650049) from The Ministry of Education, Science and Culture and by joint projects (1995–1996) between Japan Society of the Promotion of Science and the Royal Society/British Council.

References

[1] Ehrlich D J, Moulton P F and Osgood R M 1978 *Opt. Lett.* **4** 184
[2] Moulton P 1985 *Laser Handbook* vol 5, ed M Bass and M H Stitch (Amsterdam: North-Holland) p 282
[3] Blasse G and Grabmaier B C 1994 *Luminescent Materials* (Berlin: Springer)
[4] Okada F, Togawa S and Ohta K 1994 *J. Appl. Phys.* **75** 49
[5] Kodama N, Yamaga M and Henderson B 1996 *J. Phys.: Condens. Matter* **8** 3505
[6] Yamaga M, Macfarlane P I, Holliday K, Henderson B, Kodama N and Inoue Y 1996 *J. Phys.: Condens. Matter* **8** 3487
[7] Yamaga M, Yosida T, Fukui M, Takeuchi H, Kodama N, Inoue Y, Henderson B, Holliday K and Macfarlane P I 1996 *J. Phys.: Condens. Matter* **8** 10 633
[8] Oudalov J P, Daoudi A, Joubert J C, Flem G L and Hagenmuller P 1970 *Bull. Soc. Chim. Fr.* **10** 3408
[9] Shannon R D, Oswald R A, Parise J B, Chai B H T, Byszewski P, Pajaczkowska A and Sobolewski R 1992 *J. Solid State Chem.* **98** 90
[10] Yosida T, Yamaga M, Lee D, Han T P J, Gallagher H G and Henderson B 1997 *J. Phys.: Condens. Matter* **9** 3733
[11] Weger M 1960 *Bell Syst. Tech. J.* **39** 1013
[12] Pilbrow J R 1990 *Transition Ion Electron Paramagnetic Resonance* (Oxford: Clarendon)
[13] Abragam A and Bleaney B 1970 *Electron Paramagnetic Resonance of Transition Ions* (Oxford: Clarendon)
[14] Mims W B 1965 *Phys. Rev.* **140** A531
[15] Orton J W 1968 *Electron Paramagnetic Resonance* (London: Iliffe) p 119